

# Models for Low Energy Electron Beam Induced Current Experiments in polycrystalline thin film photovoltaics

Paul M. Haney<sup>1</sup>, Heayoung P. Yoon<sup>1,2</sup>, Prakash Koirala<sup>3</sup>, Robert W. Collins<sup>3</sup>, Nikolai B. Zhitenev<sup>1</sup>

1. National Institute of Standards and Technology, Gaithersburg, MD, 20889, USA

2. Maryland Nano-Center, University of Maryland, College Park, MD 20742, USA

3. Department of Physics and Astronomy, University of Toledo, Toledo, OH, 43606, USA

**Abstract** — Electron beam induced current (EBIC) is a powerful technique which measures the charge collection efficiency of electron-hole pairs generated by an electron beam. EBIC offers sub-micron spatial resolution and is naturally suited to study polycrystalline materials. Ideally, an EBIC measurement reflects the spatially resolved quantum efficiency of the solar cell. However, critical analysis of low energy EBIC data obtained on CdTe-CdS solar cells indicates that the EBIC signal is not simply proportional to the collection probability of a working device. As a step towards more quantitative analysis of EBIC measurements of these materials, we develop models of the collection efficiency which account for surface recombination in depletion regions and screening of built-in fields from carrier accumulation. We discuss how these models can be applied to obtain quantitative data on grain boundaries in polycrystalline materials.

**Index Terms** — thin film photovoltaics, electron beam induced current, surface recombination.

## I. INTRODUCTION

Quantitative determination of electronic properties at high spatial resolution is crucial for the development of high-efficiency polycrystalline solar cells. Electron beam induced current (EBIC) is a powerful technique in which electron-hole pairs are created in proximity to an exposed surface, and the carrier collection efficiency is measured as a function of excitation position [1]. EBIC is a well-established tool to measure material properties such as the bulk minority carrier diffusion length and surface recombination. High-resolution, low electron beam energy EBIC has recently become a commonly used technique to image the response of polycrystalline solar cells such as CdTe, particularly to discriminate between the properties of grain boundaries and grain interiors. These studies demonstrate a clear correlation between device preparation, power conversion efficiency, and the contrast of grain boundaries in EBIC images [2,3]. Generally, properly treated, high efficiency devices result in bright grain boundaries, while low efficiency devices result in dark grain boundaries. This correlation is most pronounced in samples prepared by focused ion beam milling (FIB). Several techniques, such as Kelvin probe and atomic force microscopy, indicate that grain boundaries in CdTe are charged, and most likely undergo type inversion such that the grain boundary core is n-type (within the bulk p-type CdTe) [4]. This results in electrostatic fields near the grain boundary core which serve to separate carriers.

It is commonly assumed that an EBIC image corresponds to a spatially resolved map of the internal quantum efficiency. We argue that this cannot be the case, simply due to the discrepancy between the device short circuit current  $J_{sc}$  and the  $J_{sc}$  implied by an EBIC image. Referring to Fig. 1, the EBIC collection efficiency (which we denote by  $\eta$ ) maximum is less than 0.13. We estimate 10 % relative uncertainty in the measured EBIC efficiency (all uncertainties are reported as one standard deviation). The dominant sources of uncertainty are from the beam current, and from the inhomogeneous material composition, which introduces uncertainty into the backscattering coefficient of the electron beam. Integrating the CdTe EBIC collection efficiency with the absorption profile of CdTe leads to a  $J_{sc}$  value of 1 mA/cm<sup>2</sup>, compared to the device  $J_{sc}$  of 23.5 mA/cm<sup>2</sup>. The reduced collection efficiency is specific to CdTe: we've observed that single crystal Si solar cells prepared by cleaving exhibit a maximum EBIC collection efficiency of 1.

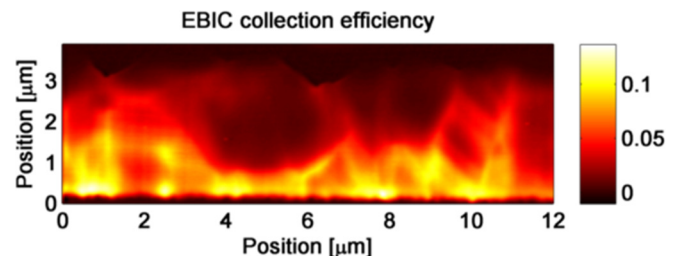


Fig. 1. EBIC collection efficiency versus beam position for a CdTe-CdS solar cell. The sample is prepared by focused ion beam milling. Note the collection efficiency varies between 0 and 0.13.

Though the EBIC image does not represent a direct map of the internal quantum efficiency, the correlation between EBIC grain boundary contrast and device performance strongly suggests that the image reveals meaningful and important material characteristics. To help uncover the information contained in EBIC images of polycrystalline solar cells, we've developed models which account for the important features of experiments performed on polycrystalline samples.

The factors which are of significance to interpreting the collection efficiency in low electron beam energy EBIC measurements include: 1. The substantial (if not dominant) role of the surface, 2. The effect of built-in electric fields on the collection probability, and 3. The possible screening of

built-in fields due to the high carrier generation rate associated with electron beam excitations. In this work we describe the theoretical development of models which include these effects. The system is inherently nonlinear, requiring “brute force” numerical methods for the general solution. Our approach is to make approximations in order to extract simple analytical expressions which are amenable to fitting experimental data. We compare the analytical expressions to numerical simulation results to check the validity of the approximations employed. We discuss how these formulas may be applied to obtain quantitative information about grain boundaries from EBIC data.

## II. MODELS

### A. The effect of surface recombination in depletion regions.

In the first section we describe the model which accounts for surface recombination in depletion regions. Traditional models of EBIC assume perfect carrier collection in depletion regions – an assumption which is clearly violated by the data of Fig. 1. Two factors point to a dominant role of surface recombination on the collection efficiency in the depletion region: 1. The maximum collection efficiency in samples prepared with FIB is significantly less than in samples prepared by cleaving, indicating that the FIB process leads to significant surface damage 2. The maximum collection efficiency increases sharply as the beam energy is increased and carriers are generated further from the surface.

Fig. 2(a) shows the geometry of the numerical model we use to explore the influence of the surface on the collection efficiency in the depletion region. The drift-diffusion equations for electrons and holes are solved together with the Poisson equation. We assume Shockley-Read-Hall recombination due to a defect level positioned at midgap. The size of the system in the  $z$ -direction ( $L_z$ ) is chosen to be large enough to ensure the results are independent of its value. See the caption of Fig. 2 for all simulation parameters. We assume a Gaussian excitation centered at the beam position  $x$  and below the surface a distance of  $z_0 = 0.3 \times R_B$ , where the excitation bulb size  $R_B$  is taken to vary with the electron beam energy  $E_{\text{beam}}$  as  $R_B = R_0 \times 0.043 (\rho_0 / \rho) \times (E_{\text{beam}}/E_0)^{1.75}$ , where  $\rho$  is the material mass density,  $\rho_0 = 1 \text{ g/cm}^3$ ,  $E_{\text{beam}}$  is the electron beam energy,  $E_0 = 1 \text{ keV}$ , and  $R_0 = 1 \text{ }\mu\text{m}$ . The variance  $\sigma^2$  of the Gaussian excitation varies with  $R_B$  as  $\sigma^2 = (R_B^2)/15$ .

Fig. 2(b) shows the calculated EBIC linescan for  $E_{\text{beam}} = 1 \text{ keV}$  and 3 values of the surface recombination velocity. The maximum EBIC collection efficiency decreases with increasing  $S$ . We find the following expression for the EBIC efficiency describes the simulation results well:

$$\eta = 1 - \left( \frac{D/z_0}{D/z_0 + \mu E} \right) \left( \frac{S/2}{S/2 + \mu E} \right) \quad (1)$$

where  $\mu$  is the carrier mobility (assumed equal for electron and holes),  $D$  is the carrier diffusivity,  $E$  is the magnitude of

the electric field (which will depend on position), and  $z_0$  is the distance of the excitation center from the surface. In (1), the first factor in parentheses represents the probability a charge located at a distance  $z_0$  below the surface will diffuse to the surface. This is given by the ratio of the diffusion velocity to the sum of the diffusion velocity and drift velocity. The second term in parenthesis is the recombination probability for a charge located at the surface. This is given by the ratio of the recombination velocity to the sum of drift and recombination velocities. The position-dependent electric field  $E(x)$  is used with (1) to predict EBIC lineshapes  $\eta(x)$ . The  $E_{\text{beam}}$  dependence of  $z_0$  results in the beam energy dependence of  $\eta$ . Figs. 2(b)-(e) demonstrate that this expression agrees well with the simulation data for a range of  $S$  and  $E_{\text{beam}}$ .

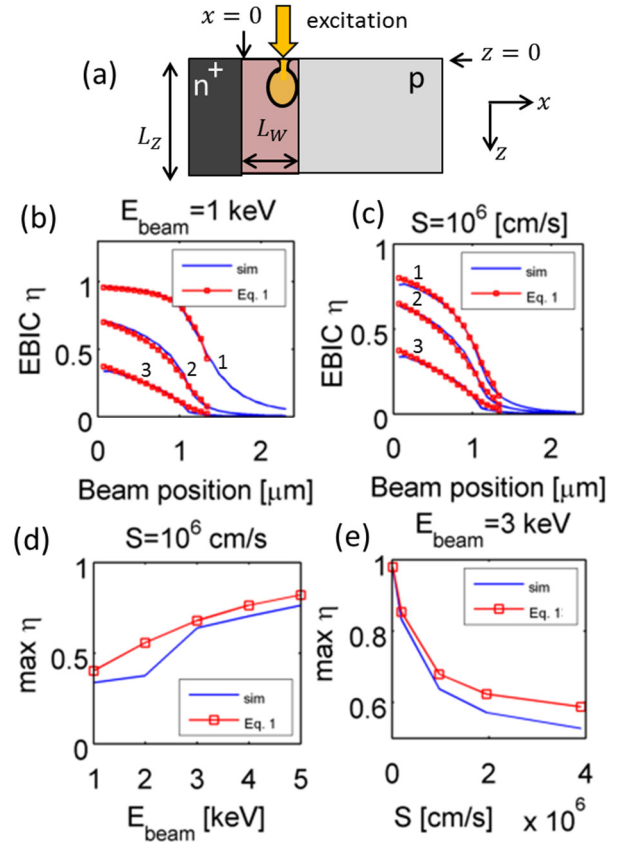


Fig. 2. (a) Model schematic of the 2-d numerical simulation of EBIC. (b) Simulation and analytical result for varying  $S$ , curves labeled 1, 2, and 3 correspond to  $S$  values of  $(2 \times 10^4, 2 \times 10^5, 10^6) \text{ cm/s}$ . (c) Simulation and analytical result for varying beam energy. Curves labeled 1, 2, and 3 correspond to electron beams of 5, 3, and 1 keV. (d) Maximum EBIC versus surface recombination velocity for fixed electron beam energy. Simulation parameters are:  $E_g = 1.5 \text{ eV}$ ,  $L_z = 15 \text{ }\mu\text{m}$ ,  $N_A = 10^{15} \text{ cm}^{-3}$ ,  $N_D = 5 \times 10^{16} \text{ cm}^{-3}$ ,  $\mu = 10 \text{ cm}^2/(\text{V}\cdot\text{s})$ ,  $\tau = 12 \text{ ns}$ ,  $\epsilon = 11$ , and selective contacts:  $S_{\text{min}} = 0$ ,  $S_{\text{maj}} = 10^6 \text{ cm/s}$ .

An important feature of Eq. (1) is that the concavity of the lineshape in the depletion region is downward. In contrast,

it's known that in the neutral region – where traditional models of EBIC apply – the concavity is upward [4]. The downward concavity in the depletion region follows from the monotonically decreasing magnitude of the electric field there. Fitting the concave downward portion of the EBIC lineshape at different beam energies and allows for an estimation of  $S$  and  $E(x)$ . This procedure may be used to map out the field distribution of the p-n junction, and the fields surrounding isolated grain boundaries.

### B. Screening of internal fields due to high carrier generation rate

We next describe a model which accounts for the screening of built-in fields due to the high generation rate associated with electron beam excitation. An electron with energy  $E_{\text{beam}}$  generates approximately  $E_{\text{beam}}/(3 \times E_g)$  free electron-hole pairs, where  $E_g$  is the material band gap. The range of excitation is given by  $R_B$ , as described in the last section. For an electron beam current of 200 pA and energy  $E_{\text{beam}} = 5$  keV, the generation rate density exceeds that of 1 sun illumination by a factor of  $10^5$ . This indicates that it is possible to drive the system into a nonlinear regime, by inducing large nonequilibrium carrier concentrations which screen the build-in fields.

Generally, screening is important when the total carrier generation rate  $G$  exceeds the maximum current which is accommodated by the p-n junction. In a one-dimensional description, this maximum current is  $q\mu N_A V_{bi}/L$ , where  $q$  is the electron charge,  $\mu$  is the majority carrier mobility,  $N_A$  is the doping,  $V_{bi}$  is the built-in potential of the p-n junction, and  $L$  is the absorber thickness. In this case, the maximum current is the product of the material conductivity with the built-in electric field. In an EBIC experiment, carriers are generated in a small region of three-dimensional space inside a material. This alters the electrostatics relative to the one-dimensional description, as described in detail in Ref. [6]. In three dimensions, the critical generation rate scales as  $q\mu N_A V_{bi} L$ .

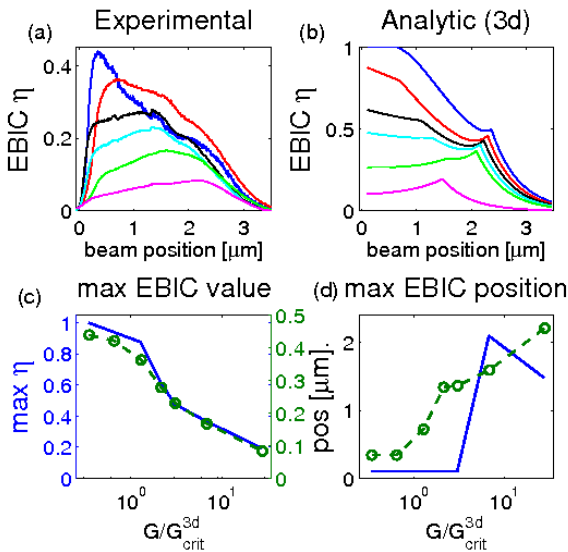


Fig. 3. (a) shows experimental EBIC profiles for CdTe with electron beam energy of 5 keV, and electron beam currents of (26, 97, 162, 231, 516, and 2110) pA (in blue, red, black, cyan, green, and purple, respectively). (b) shows the analytical model lineshape for the same set of beam current values, with  $\mu N_A = 1.2 \times 10^{14} \text{ (cm} \cdot \text{V} \cdot \text{s)}^{-1}$ ,  $V_{bi} = 1.5 \text{ eV}$ , and  $L_D = 500 \text{ nm}$ . (c) dashed green curve shows the experimental maximum EBIC efficiency as a function of total generation rate (scaled by critical generation rate, taken experimentally from letting  $I_{\text{crit}} = 70 \text{ pA}$ .) Solid blue line is the same result for the analytical model. Note the experimental (analytic) y-axis is on the left (right). (d) dashed green curve shows the experimental position of the EBIC maximum, while the solid blue line is the analytical model.

We omit a detailed derivation of the form of the EBIC lineshape in the screened regime. To give a flavor of the model, we offer the following qualitative description of the important ingredients: We assume that the carriers accumulate and screen the built-in electric field. We denote the length scale over which fields are screened by  $R^*$ . We assume charges diffuse and recombine within the screened volume (a sphere of radius  $R^*$ ), while charges which diffuse to the edge of the screened region are collected. Setting the total charge generated equal to the sum of the recombination and collected current leads to an implicit equation for the screening length  $R^*$ , from which the EBIC collection efficiency may be determined.  $R^*$  satisfies:

$$\frac{GR^*}{\sinh(R^*/L_D)} - \frac{2\pi\mu V_{bi} N_A L}{1-R^*/L} = 0 \quad (2)$$

where  $L_D$  is the diffusion length.

Fig 3(a) shows experimental EBIC lineshapes for increasing electron beam current. As before, we estimate 10 % relative uncertainty in the measured EBIC efficiency amplitude. The uncertainty in the magnitude of the EBIC signal therefore has little influence on the uncertainty of the shape. This is because the length scale for this material inhomogeneity (e.g. alloying) is much smaller than the electron beam spot size, so that this source of error is uniform across linescans. We estimate an uncertainty in the maximum position of 50 nm based on the discretization of the electron beam position in the linescan. Fig. 3(b) shows the corresponding lineshape derived from (2). The model provides the qualitative features of the EBIC lineshapes as one enters the screening regime: the maximum of the EBIC profile moves away from the p-n junction into the middle of the device, and the peak broadens out substantially. Additionally, the maximum value of the EBIC efficiency drops. By varying the beam current and studying the trend of these quantities, the presence of screening may be detected, and the EBIC lineshapes may be interpreted appropriately. The model also provides guidance for the onset of the screening regime: when the total generation rate exceeds  $G_{\text{crit}}^{3d} = q\mu N_A V_{bi} L$ , screening effects become important.

### III. CONCLUSIONS AND OUTLOOK

To summarize, we present two models which apply to EBIC experiments on polycrystalline solar cells. Using the fact the collection efficiency is always below 1, we develop a model which described carrier collection efficiency in depletion regions which may be applied to extract the structure of built-in fields near grain boundaries. Additionally, we develop a model that accounts for screening effects which may be important for thin film photovoltaic response to electron beam excitation.

### REFERENCES

- [1] J. I. Hanoka, and R. O. Bell, "Electron-Beam-Induced Currents in Semiconductors", *Ann. Rev. of Mat. Sci.*, vol. 11, 353-380 (1981).
- [2] C. Li, Y. Wu, J. Poplawsky, T. J. Pennycook, N. Paudel, W. Yin, S. J. Haigh, M. P. Oxley, A. R. Lupini, M. Al-Jassim, S. J. Pennycook, and Y. Yan, "Grain-Boundary-Enhanced Carrier Collection in CdTe Solar Cells", *Physical Review Letters*, vol. 112, 156103-1-5 (2014).
- [3] Heayoung P. Yoon, Paul M. Haney, Dmitry Ruzmetov, Hua Xua, Marina S. Leite, Behrang H. Hamadani, A. A. Talin, N. B. Zhitenev, "Local electrical characterization of cadmium telluride solar cells using low-energy electron beam", *Sol. En. Mat. And Sol. Cells*, vol. 117, 599-504 (2013).
- [4] I. Visoly-Fisher, S. R. Cohen, K. Gartsman, A. Ruzin, and D. Cahen, "Understanding the Beneficial Role of Grain Boundaries in Polycrystalline Solar Cells from Single-Grain-Boundary Scanning Probe Microscopy" , *Adv. Func. Mat.*, vol. 16, 649-660 (2006).
- [5] W. Van Roosbroek, "Injected Current Carrier Transport in a Semi-Infinite Semiconductor and the Determination of Lifetimes and Surface Recombination Velocities", *J. App. Phys.* Vol. 26, 380-391 (1955).
- [6] P. M. Haney, H. P. Yoon, P. Koirala, R. W. Collins, N. B. Zhitenev, "Electron beam induced current in the high injection regime", arXiv:1410.4435v1, (2014).